



Cite this: *J. Mater. Chem. C*, 2021,
9, 3555

Highly ordered smectic structures of disc–rod luminescent liquid crystals: the role of the tolane group†

Yurong Liu,^{ab} Wei Li,^a Xuan Zhou,^{cd} Wai-Yeung Wong^{id}*^{cd} and
Zhen-Qiang Yu^{id}*^a

Two novel calamitic tolane luminogen-modified triphenylene-based discotic luminescent liquid-crystals (LLC) were rationally designed and synthesized to investigate the self-assembly competition between triphenylene discogens and tolane calamitic mesogens. The results show that the LLCs formed thermodynamically stable highly ordered smectic B or smectic E phase as well as lamellar crystal structures, instead of the traditional columnar phase. The photoluminescence properties, which changed according to crystal structures, were also studied, indicating the important role of the tolane group in manipulating the self-organization of disc–rod molecules and consequently achieving enhanced emission.

Received 28th November 2020,
Accepted 4th February 2021

DOI: 10.1039/d0tc05608a

rsc.li/materials-c

1 Introduction

The phase structures and phase transitions of self-assembled organic materials have not only been governing the principles in fundamental science but they have also formed the basis of material multifunctionalities.^{1–4} Engineering molecular self-assembly on the nanometer or micron scale is an important approach for tailoring solid-state microstructures and developing new functional materials.^{5–7} There has been a resurgence of research on the self-assembly behavior of classical discogen triphenylene due to the current development of nanoscience, particularly in thermo- or electro-conducting systems.^{8–14} Due to the largely π -conjugated planar structure, the self-organized nanostructures of triphenylene-based molecules are usually limited to hexagonal or rectangular columnar structures dominated by strong π - π interactions between the π -conjugated planar discogens.¹⁵

There have been numerous efforts devoted to manipulating the self-assembly of discotic liquid crystal (DLC) molecules.^{16,17} Apart from constructing hierarchical structures to maintain the columnar structure, breaking the disc packing is another approach to vary the self-organized structures.¹⁸ It has been reported that by taking the advantages of the steric hindrance effect, modification of the triphenylene unit with bulky groups could achieve the nematic phase.¹⁹ When six cyanobiphenyl calamitic mesogens were chemically linked to the periphery of the triphenylene discogen through twelve methylene units, benefiting from the decoupling of the two components (rod and disc mesogens), the resultant molecule formed a biaxial nematic phase with the optical director of the cyanobiphenyl group orthogonal to the discotic mesogen.^{20,21} Additionally, introducing rodlike mesogens to the periphery of the discotic skeleton through rational selection of the spacer and regulating the interactions between triphenylene mesogens and between the pending calamitic mesogens can also be a promising dual-component strategy.

Shape-induced phase segregation of disc–rod molecules has been studied to form the smectic A (SmA) or smectic C (SmC) phase.^{22,23} In addition, triphenylene modified with rod-shaped photo-isomerized peripheries has been reported to show thermal- and photoinduced phase transitions and can exhibit the thermodynamically metastable SmA state.^{24–26} However, to the best of our knowledge, the thermodynamically stable, highly ordered smectic phase has never been reported.

In this communication, we designed and synthesized two DLCs with six tolane mesogenic groups attached to the 2,3,6,7,10,11 positions of triphenylene, and the name can be

^a School of Chemistry and Environmental Engineering, Low-Dimensional Materials Genome Initiative, Shenzhen University, Shenzhen 518071, China.
E-mail: zgyu@szu.edu.cn

^b Department of Chemistry and Materials Science, University of Science and Technology of China, Hefei, 230026, China

^c Department of Applied Biology and Chemical Technology, The Hong Kong Polytechnic University, Hung Hom, Hong Kong, China
E-mail: wai-yeung.wong@polyu.edu.hk

^d The Hong Kong Polytechnic University Shenzhen Research Institute, Shenzhen Virtual University Park, Nanshan District, Shenzhen 518057, China

† Electronic supplementary information (ESI) available: The characterization of molecules and calculation methods. See DOI: 10.1039/d0tc05608a

abbreviated as **DR-5** and **DR-7** (hereafter collectively called **DRs**, where D denotes the discotic triphenylene group, R denotes the rodlike tolane mesogenic group, and 5 or 7 is the alkyl tail length). Such a study is able to illustrate an effective strategy towards thermodynamically stable, functional, highly ordered smectic nanostructures. That is, this can trigger the competition between the packing of rods and discs by elaborately designing the spacer and rod periphery. The resultant LLCs bear novelty not only with regard to the thermodynamically stable highly ordered smectic phase structures formed but also for the synergistic effect of rods and discs in achieving enhanced luminescence. This study elucidates the role of tolane as mesogen and luminogen in disc-rod molecules.

2 Results and discussion

2.1 Structural design

The chemical structures of **DR-5** and **DR-7** are displayed in Fig. 1. The six tolane mesogens are covalently linked to the triphenylene core through six methylene units. Here, there is a very crucial impact of the six-methylene spacer on the coupling dynamics of the two mesogens. Moreover, tolane can also act as a luminogen to achieve versatile functions.^{27,28} Additionally, the alkyl tail length influences the molecular mesophase behavior, as we previously demonstrated.^{29,30} The target molecules are prepared by the route depicted in Scheme S1 (ESI[†]). The tolane groups are embedded into the skeleton of triphenylene by the nucleophilic substitution reaction of hexahydroxytriphenylene (**10**) with **R-5** and **R-7** (hereafter collectively called **Rs**). It was found that the collected powdery **DRs** are blue emissive, as shown in Fig. 1. The phase behaviors were investigated by differential scanning calorimetry (DSC), polarized optical microscopy (POM), and temperature-dependent wide-angle X-ray diffraction (WAXD). Interestingly, the **DRs** can form a stable highly ordered smectic phase instead of the traditional columnar structure due to the overwhelming strong interaction between tolanes over the interaction between the triphenylene rings.

2.2 Characterization

A DSC trace of **DR-5** (Fig. 2a) shows three exothermic peaks at 65, 57, and 35 °C on cooling at a scan rate of 5 °C min⁻¹,

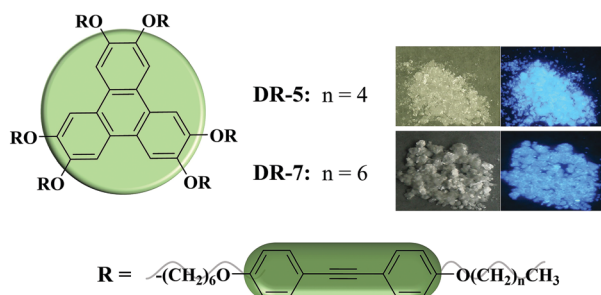


Fig. 1 Chemical structures of **DR-5** and **DR-7** (the structures of triphenylene and tolane are respectively modelled as disc and rod) and photographs of them in solid-state under sunlight and ultraviolet (UV) light, respectively.

whereas only one endothermic peak at 72 °C is recorded on heating, implying a monotropic LC transition. The transition at 35 °C can be assigned to a LC to crystal transition. The other two transitions at 57 and 65 °C are associated with the transitions of LC-LC and LC-isotropic phases. Interestingly, **DR-7**, with a chemical structure that is similar to **DR-5**, exhibits quite different phase transition behavior. Two sets of peaks are detected during cooling and subsequent heating cycles, suggesting the enantiotropic nature of **DR-7**. The transition temperature at 75 °C during cooling is very close to that at 77 °C during heating, indicating a thermodynamic equilibrium, which is associated with LC phase transitions.³¹ In contrast, the transition at lower temperature shows supercooling of 15 °C, which can be assigned to the LC-crystal phase transition.

POM was applied to observe the textures of **DRs**. When observed under POM, **DR-5** shows a focal conic texture (Fig. 2b and Fig. S1, ESI[†]) upon cooling from the isotropic liquid to 63 °C, indicative of the smectic mesophase formation. By continued cooling to 55 °C, another focal conic texture was observed, reflecting that another smectic phase or other very similar phase was formed. By further lowering the temperature, crystallization occurs. For **DR-7**, the POM microphotograph also clearly depicts the emerged focal conic texture in the heating and cooling procedures at 75 °C as shown in Fig. 2b and Fig. S1 (ESI[†]). The POM observations are consistent with their corresponding DSC results, confirming the LC phase transitions. The difference in phase transition behaviors between **DRs** implies that the minor disparity in alkyl tail lengths could exert a strong effect on the molecular packing behavior.

WAXD was performed to obtain insights into the molecular packing in different mesophases. Fig. 2c shows the diffraction patterns of **DRs** at the LC state collected upon cooling from isotropic melts. For **DR-5**, when cooled to 60 °C, a very strong and a very weak peak at 2θ of 2.89° and 5.76° with a d -spacing ratio of 1 : 1/2 were collected in the low-angle region, indicating a layered structure with a layer thickness of 3.06 nm, while in the wide-angle region, a sharp and intense reflection at 2θ of 20.6° with a d -spacing of 0.43 nm and a broad scattering halo centered at approximately 20° were detected. This unveils the long-range ordered packing of tolane groups on a sub-nanometer scale and the amorphous packing of the alkyl tails, indicative of a smectic B (SmB) phase of **DR-5** rather than a hexatic B phase, which only revealed short-range ordering on a sub-nanometer scale.³²

By further cooling to 50 °C, three reflections with a d -spacing ratio of 1 : 1/2 : 1/3 were detected in the low-angle region, clearly rendering a highly ordered smectic LC phase with a layer thickness of 1.87 nm. Two fresh reflections at 2θ of 23.58° and 25.35° in the high-angle region emerged, which is highly reminiscent of the birth of a smectic E (SmE) phase, and suggests that the hexagonally packed molecular packing model of tolane groups on the sub-nanometer scale is transformed to a rectangular one.^{33–35} The three peaks labeled 1', 2', and 3' can be assigned as (110), (200), and (210) diffractions, respectively, of the SmE phase on a sub-nanometer scale with $a' = 0.75$ nm,

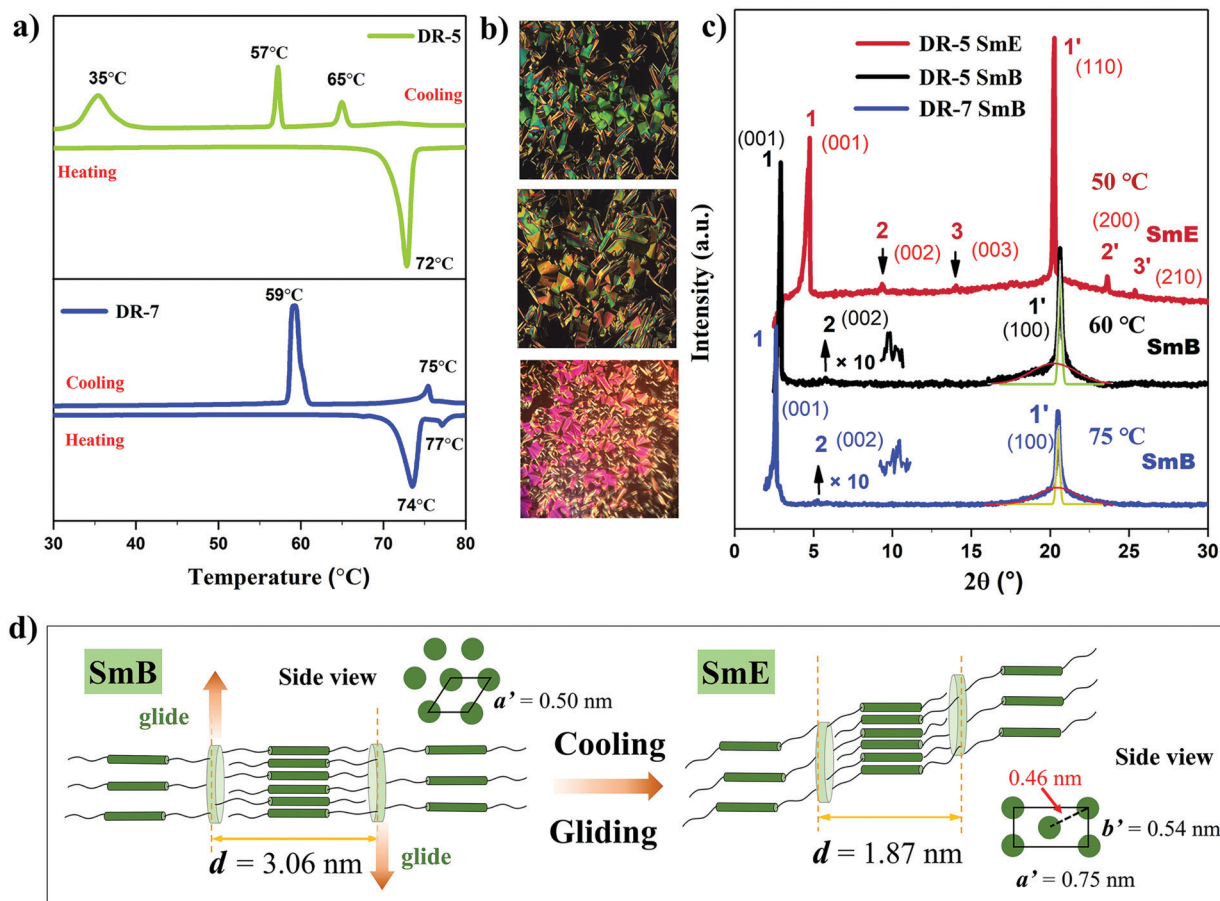


Fig. 2 (a) DSC traces of DRs detected upon cooling and subsequent heating with a scan rate of $5\text{ }^{\circ}\text{C min}^{-1}$. (b) POM textures of DR-5 observed at $63\text{ }^{\circ}\text{C}$ (top), $55\text{ }^{\circ}\text{C}$ (middle), and that of DR-7 at $75\text{ }^{\circ}\text{C}$ (bottom) upon cooling from isotropic melts with a cooling speed of $1\text{ }^{\circ}\text{C min}^{-1}$. (c) The WAXD patterns of DRs at different mesophases. (d) Schematic illustration of the molecular packing models of DR-5 in SmB and SmE phase and side views of the models along the tolane mesogens.

$b' = 0.54$ nm, and $\gamma = 90^{\circ}$. Therefore, the average area occupied by each tolane group of DR-5 in the $a'b'$ plane is approximately 0.20 nm^2 (i.e., $a'b'/2$), which matches the reported value well.^{34–36} The sharpness of reflections 1 and 1' illuminates the long-range correlation of the interlayer and intralayer orders, respectively. It is also noted that the sharp peak at $57\text{ }^{\circ}\text{C}$ detected during DSC trace is commonly associated with the mesophase with a high degree of orders.¹⁷ The DSC data offer further support upon the WAXD analysis.

Briefly, DR-5 can sequentially form SmB and SmE phases before crystallization with a layer thickness of 3.06 nm in SmB phase, which is much larger than that of 1.87 nm in SmE phase. By contrast, DR-7 also exhibits a smectic B phase when cooled to $75\text{ }^{\circ}\text{C}$, but reflection 1 shifts to a lower angle region with a lamellae thickness 0.3 nm thicker than that of DR-5, which is approximately the extended length of four methylene units, indicating that the alkyl tails have assumed an extended conformation and dominate the lamellae thickness. Additionally, DR-7 forms the enantiotropic LC phase, and the SmB phase cannot be further developed into the SmE phase during cooling. These phenomena indicate that the phase structures are partially dependent on the alkyl tail length. It is also worth noting that the

characteristic diffraction at 2θ of approximately 25° of the ordered face-on stacking of triphenylene discogen through intermolecular π - π interaction is absent in both WAXD patterns of SmB and SmE phase of DR-5, indicating that the SmB-SmE transition can be assigned to a further ordering of the tolans. These observations strongly suggest that the tolane mesogens preferentially bundle to form a layer and dominate the molecular packing structure, although this hinders the traditional ordered packing between triphenylene discogens.

What is the driving force behind these different molecular packing models? It may include molecular shape and space-filling effects. Based on the above analysis, the proposed molecular packing models for DR-5 are schematized in Fig. 2d. The peripheral tolane groups are alternately assigned on both sides of the triphenylene plane and aligned to produce a layered phase structure. In both molecular packing models, the tolane groups acquire an interdigitated packing manner. When the temperature decreases, the d -spacing on the nanometer or sub-nanometer scale will be slightly shrunken. However, the lateral shrinkage ratio in the tolane region and alkyl tail region is different: the loosely packed alkyl tail region will be squeezed by the closely packed tolane region, and the

different shrinkage ratio of the different regions will lead to a slight gliding of the tolane region along the lateral direction. This slight lateral glide decreases the layer thickness and also changes the packing model of the tolane group from a two-dimensional hexagonal lattice to a rectangular one.

2.3 Self-assembly of the disc-rod molecules

The self-assembly of **DRs** in crystal phase was further investigated. The inset of Fig. 3a shows a scanning electron microscopy (SEM) image of the layered morphology of **DR-5** prepared from solvent evaporation of tetrahydrofuran (THF) solution, indicating the layered structure in the crystal phase. A sheet-like morphology with large domain sizes are unveiled for both **DRs** and **Rs** (Fig. S2, ESI[†]). In contrast, methoxy- or hydroxy-substituted triphenylene compounds **9** and **10**, as referential molecules, exhibit distinct bulk morphologies, which should be attributed to the π - π stacking of the triphenylene cores. Fig. 3a and Fig. S4a (ESI[†]) show the powder WAXD patterns of **DR-5** and **DR-7** in the crystal state, respectively.

The reflections in the small-angle region of **DR-5** with a *d*-spacing ratio of 1/2 : 1/3 : 1/4 : 1/5 : 1/6 : 1/7 : 1/8 : 1/9 and the multi-reflections in the wide-angle region confirm the prominent layered crystal structure, implying the further ordering of the dominated rods from LC phases. The lamellar structures of **Rs** are also revealed in Fig. S3 (ESI[†]), which is in accordance with the SEM images. The low-angle diffraction patterns of **Rs** are very similar to those of **DRs**, which can be considered for the indication of the governance of tolane groups in the self-organization of **DRs**. Their difference in the wide-angle region describes the effect of the triphenylene core on guiding molecular packing. Because it is very difficult to obtain suitable single crystals of **DRs** to conduct a single-crystal diffraction study, structural refinement was applied to obtain the crystal structure of **DRs**.

The refinement data indicate that two monoclinic systems exist ($P2_1/c$ space group), with $a = 5.2$ nm, $b = 0.48$ nm, and $c = 1.7$ nm ($\alpha = \gamma = 90^\circ$ and $\beta = 94.3^\circ$) for **DR-5** and $a = 5.6$ nm, $b = 0.48$ nm, and $c = 1.7$ nm ($\alpha = \gamma = 90^\circ$ and $\beta = 93.5^\circ$) for **DR-7**

(Table S1 and Fig. S5, ESI[†]). Increasing the tail length leads to an increase in the *a* dimension of the unit cell, but no change in the *b* and *c* dimensions, suggesting that the alkyl tails as well as tolane groups and spacers are orientated along the *a*-axis. Additionally, a longer tail also gives rise to larger layer thickness of the smectic phase, as aforementioned. The formed lamellae should stack in parallel to the *bc* plane and subsequently perpendicular to the orientation of the tolane groups. Assuming that all the spacers and alkyl tails adopt all-*trans* conformations, the molecular sizes of the core and tolane components are calculated *via* the geometrical optimization method by density functional theory (DFT).

The tolane motif (containing the spacer and alkyl tail) for **DR-5** shows a length of approximately 2.67 nm, while the discotic core exhibits a diameter of approximately 1.2 nm (that is the *D* value) (Fig. 3b). Then, the molecular length of **DR-5** (Fig. 3c) is calculated to be 5.2 nm (5.7 nm for **DR-7**), well matching the *a* dimensions of the corresponding unit cells. The *b* dimension of the unit cell (0.48 nm) is comparable to the lateral distance of the tolane mesogen (0.50 nm in SmB and 0.54 nm in SmE). Hence, the crystal structure of **DRs** is illustrated as the schematic drawing shown in Fig. S4b (ESI[†]) (viewed along the *b* axis), wherein the triphenylene cores and tolane groups are modelled as discs and rods, respectively, and are chemically linked through flexible spacers.

Why do **DRs** form a highly ordered smectic phase, and what role does the tolane mesogen play during the LC phase formation? There would be competition between the tolane groups and the triphenylene cores for the factor that governs the self-assembly due to the coupling of the dynamics of the two mesogens. However, according to the optimized geometry, the triphenylene core is slightly distorted, and the planarity is broken. Thus, the interdigitated packing of tolane groups will predominantly form a 2D arrangement parallel to the *bc* plane, while the triphenylene discs are intercalated, preventing the π - π stacking of the triphenylene core to form face-on stacked columns. In this context, **DRs** can exhibit ordered smectic LC phases without the co-existence of a columnar structure.

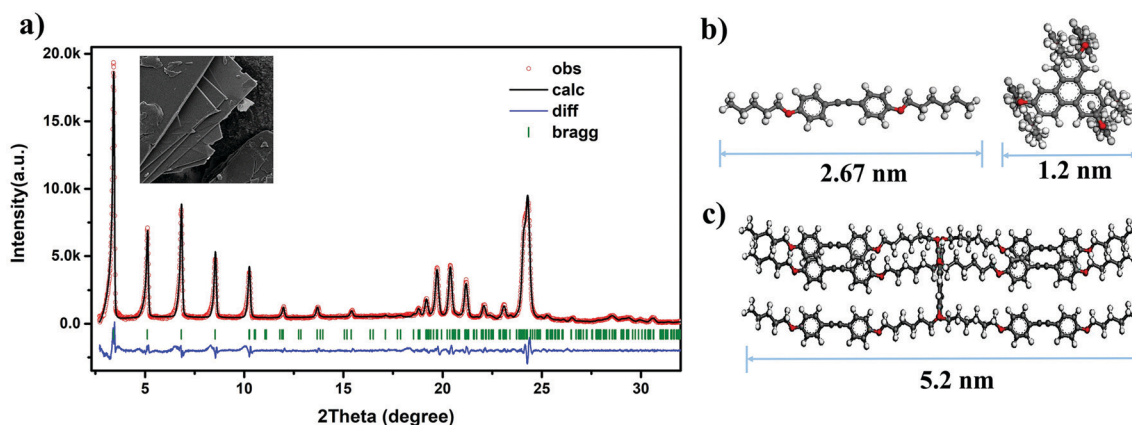


Fig. 3 (a) The refinement of the powder WAXD pattern of **DR-5** in crystal phase. The inset shows the corresponding SEM morphology. The observed and the calculated profile perfectly overlapped, and the difference plot shown at the bottom is also very small. The calculated molecular sizes of the (b) tolane motif (containing the spacer and alkyl tail) (left) as well as the triphenylene core (right) and (c) **DR-5**.

However, it was found in our previous study that the tolane-based calamitic LC molecule could form SmC or SmB phase.²⁷ Thus, the triphenylene core here may behave as an anchor for tolane mesogens, and may exert a synergistic effect on the self-assembly of tolane groups to construct a highly ordered smectic phase with additional ordering on the sub-nanometer scale.

According to the crystal stacking model, the average area occupied with each tolane group within the discotic plane can be calculated to be $(1/4 \times \pi D^2)/6 = 0.19 \text{ nm}^2$ (D denotes the diameter of the triphenylene core), which is slightly smaller than that in SmB (0.22 nm^2) and SmE (0.20 nm^2) phase and indicative of the close packing of the tolane in the crystal state. The proposed stacking model also could provide a reasonable explanation regarding the effect of alkyl tails on the packing of tolane groups (as demonstrated in Fig. S4c, ESI[†]). For DR-5, the spacer is slightly longer than the alkyl tail, and this results in an almost full contact with the tolane groups of the neighboring molecules and subsequent strong interaction between the tolane groups. Increasing the tail length, as in DR-7, will lead to less contact and thereby weakened interaction. In this context, compared with DR-5, DR-7 exhibits a larger layer thickness in SmB phase and cannot be further developed into the highly ordered SmE phase, which also may lead to the lower quantum yield compared to DR-5 (*vide infra*).

2.4 Photoluminescence of the disc-rod molecules

Aggregation-induced emission (AIE)-active LC materials are promising candidates for high-performance luminescent liquid crystals (LLC), as they are completely free of aggregate-caused quenching (ACQ) during the fabrication of solid-state devices. Therefore, it is interesting to investigate the heredity and variation behavior when embedding the tolane, also a typical AIEgen, into a self-organized system. It was found that DRs are non-emissive in solution but emit blue light in the solid state under UV illumination, suggesting their AIE activity. The luminescent properties were studied in THF/water mixtures with different water fractions (f_w), where THF is a satisfactory solvent, and water is a poor solvent for all samples.

Taking DR-5 as an example, the absorption spectrum (Fig. S6a, ESI[†]) is not a simple combination of the corresponding moieties R-5 and 9. With f_w increasing from 0% to 99%, the emerged fresh peak and enhanced intensity in the UV-Vis absorption spectra could be attributed to the scattering effect of in situ-generated nanoaggregates.³⁷ The recorded photoluminescence (PL) spectra (Fig. S7a–d, ESI[†]) also indicate that DRs and Rs are AIE active. Additionally, the similarity in PL spectra between DRs and Rs indicates that the luminescence properties of DRs are mainly inherited from the inserted tolane group. The PL intensity at the maximum emission wavelength is boosted by different times upon aggregation: with f_w increasing from 0% to 99%, the emission enhancement for DRs is more obvious than that for Rs, which can be concluded from Fig. S7e (ESI[†]).

Because tolane groups exhibit crystal-induced emission,¹³ the above observations strongly imply that the triphenylene cores have a positive effect on the alignment of peripheral

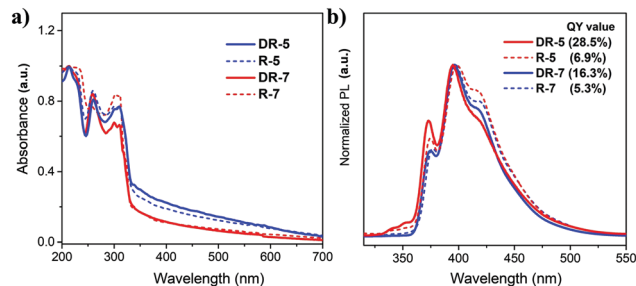


Fig. 4 (a) Absorption and (b) PL spectra of DRs and Rs in the solid-state. The photoluminescence quantum yields of DRs and Rs are indicated in (b).

tolane groups to form more ordered molecular stacks instead of disordered nanoaggregates. The noticeable increase in quantum yield (QY) in the crystal state provides further evidence for this. The QY value of 6.9% for R-5 dramatically increased to 28.5% after the chemical attachment of R-5 to the triphenylene core to form DR-5. The QY value of 16.3% for DR-7 is much smaller than that of DR-5, and it may be caused by the decreased contact of tolane groups during molecular packing. The excitation and absorption spectra were also simulated by time-dependent density functional theory (TD-DFT) using Gaussian at the B3LYP/6-31G(d) level. The obtained computational absorption spectra are displayed in Fig. S6c (ESI[†]).

The calculated maximum absorption wavelength of compound R is at approximately 300 nm, which is close to that of the target DR but redshifted compared with compound 9 (by approximately 225 nm). Additionally, the calculated spectrum of DR is not a simple overlay of that of compounds 9 and R. These results match well with the experimental data. The optimized geometries and the main molecular orbitals involved are shown in Fig. S6d–f (ESI[†]), which show that for the components Rs and compound 10, both the HOMO and LUMO orbitals are distributed on the entire molecules, indicating the large π -conjugation. In contrast, the HOMO orbital of DRs is distributed in the peripheral tolane group, while the LUMO orbital is contributed by both the triphenylene core and tolane side substituents. This indicates that the coupling between the two components occurs not only upon molecular self-assembly but also in molecular orbital formation, where the tolane moiety shows a dominant effect.

The solid-state UV-Vis and PL spectra are plotted in Fig. 4a and b, also depicting the domination of the tolane component over the optical properties of DRs. The photographs of DRs and Rs recorded during heating and cooling processes under sunlight and UV light are vividly contrasted in Fig. S8 (ESI[†]) to further illustrate the enhanced photoluminescence of DRs caused by the ordered molecular self-organization.

3 Conclusions

Through rational modification of the periphery of the discotic triphenylene molecule with calamitic tolane luminogens, two AIE-active LLC materials, DR-5 and DR-7, which exhibit the desired thermodynamically stable highly ordered smectic

phases, were successfully achieved for the first time. The LC phase structures and phase transitions were studied. The sheet-like morphologies were confirmed by SEM images, and the lamellar molecular structures were determined by WAXD patterns. The absence of the typical columnar stacking of the triphenylene-based discogen occurs in both mesophase and crystal state, as a result of the dominant packing of tolan over the stacking of discotic triphenylene. A stacking model is proposed to satisfy the experimental observations. Taking advantage of the ordered molecular packing, DR-5 and DR-7 exhibit an enhanced AIE effect, with respect to the corresponding tolan-based molecules R-5 and R-7. The study presented here evidently illustrates a feasible strategy towards manipulating molecular self-organization by rationally introducing a functional motif and subsequently promoting its performance.

4 Experimental

4.1 Synthetic procedures

Synthesis of DR-5. Hexahydroxytriphenylene (0.16 g, 0.4 mmol) and dried KOH (0.25 g, 3.6 mmol) were placed in an oven-dried flask. After three cycles of pumping and purging with N₂, compound R-5 (1.42 g, 3.2 mmol) dissolved in 15 mL of anhydrous dimethylformamide (DMF) was slowly injected into the mixture. The mixture was heated to 100 °C and allowed to react for 72 h. The mixture was poured into 50 mL of water, and the crude product was filtered and purified by column chromatography, which afforded the product in a yield of 20%. ¹H NMR (400 MHz, CDCl₃), δ (TMS, ppm): 8.06 (s, 6H), 7.44 (d, *J* = 8.0 Hz, 24H), 6.86 (d, *J* = 8.0 Hz, 24H), 4.19 (t, *J* = 4.0 Hz, 12H), 3.98 (td, *J* = 8.0 Hz, 4.0 Hz, 24H), 1.82–1.69 (m, 36H), 1.48–1.35 (m, 48H), 0.93 (t, 18H). ¹³C NMR (400 MHz, CDCl₃) δ: 161.38, 159.13, 133.05, 115.76, 115.42, 114.70, 88.16, 68.27, 67.98, 64.13, 29.20, 28.94, 28.66, 28.39, 25.88, 22.57, 14.28; MALDI-TOF-MS (*m/z*): [M + H]⁺ calculated for C₁₆₈H₁₉₃O₁₈, 2499.4142. found, 2499.4120.

Synthesis of DR-7. DR-7 was synthesized by similar procedures that were used to obtain DR-5, while compound R-7 (1.51 g, 3.2 mmol) was used to obtain a white solid in a yield of 22%. ¹H NMR (400 MHz, CDCl₃), δ (TMS, ppm): 8.05 (d, 6H), 7.43 (d, *J* = 8.0 Hz, 24H), 6.83 (d, *J* = 8.0 Hz, 24H), 4.16 (t, *J* = 4.0 Hz, 12H), 3.94 (td, *J* = 8.0, 4.0 Hz, 24H), 1.81–1.72 (m, 24H), 1.46–1.30 (m, 72H), 0.89 (t, *J* = 8.0 Hz, 18H). ¹³C NMR (400 MHz, CDCl₃) δ: 161.33, 159.09, 133.01, 115.72, 115.70, 114.65, 88.15, 68.23, 67.93, 64.07, 31.97, 29.90, 29.33, 29.30, 28.63, 26.18, 25.85, 22.80, 14.28. MALDI-TOF-MS (*m/z*): [M + H]⁺ calculated for C₁₈₀H₂₁₇O₁₈, 2667.6020; found, 2667.6101.

4.2 Computational simulation

The WAXD refinement profiles were obtained through Le Bail refinement. Computer modelling was conducted to obtain the data on the molecular size. A single molecule of DR containing six tolan groups, one triphenylene core, and six alkyl spacers and six alkyl tails was constructed by Materials Studio (Accelrys). We further assumed that the spacers and the alkyl

tails were all in the *trans* conformation. The geometry optimization was conducted using a quantum chemistry method (DFT) and the Dmol3 model in Materials Studio. The PW31 model in Generalized Gradient Approximation (GGA) was used for exchange–correlation energy calculations.

To study their optical properties, the energy optimization calculations for the tolan group, triphenylene group, and the final target compound (named compound 7', 9, and DR', respectively) were individually conducted. To simplify the calculation, the alkyl spacers and tails were rationally represented by methyl units. Geometry optimization was performed using Gaussian D 01 at D 01 at the B3LYP/6-31G level while UV-Vis absorption spectra were calculated for 30 states using TD-DFT at D 01 at the B3LYP/6-31G level.

Conflicts of interest

There are no conflicts to declare.

Acknowledgements

This work was financially supported by the National Natural Science Foundation of China (No. 21875143 and 21674065), the Innovation Research Foundation of Shenzhen (No. JCYJ20180507182229597 and JCYJ20170817100547775), and the Natural Science Foundation of Guangdong Province (No. 2016A030312002). W.-Y. W. would like to thank the Science, Technology and Innovation Committee of Shenzhen Municipality (JCYJ20180507183413211), the Hong Kong Research Grants Council (PolyU 123384/16P), Hong Kong Polytechnic University (1-ZE1C), and the Endowed Professorship in Energy from Ms Clarea Au (847S). Y. Liu and X. Zhou would like to thank the China Postdoctoral Science Foundation Funded Project (2020M672817 and 2019M653007). The theoretical calculations described in this article were supported by the High-Performance Cluster Computing Centre of Hong Kong Baptist University, which receives funding from the Research Grants Council, University Grants Committee of the HKSAR. Special thanks to the Instrumental Analysis Center of Shenzhen University (Xili Campus).

Notes and references

- 1 T. Kajitani, K. Motokawa, A. Kosaka, Y. Shoji, R. Haruki, D. Hashizume, T. Hikima, M. Takata, K. Yazawa, K. Morishima, M. Shibayama and T. Fukushima, *Nat. Mater.*, 2019, **18**, 266–272.
- 2 J. Huang, Z. Su, M. Huang, R. Zhang, J. Wang, X. Feng, R. Zhang, R. Zhang, W. Shan, X.-Y. Yan, Q.-Y. Guo, T. Liu, Y. Liu, Y. Cui, X. Li, A.-C. Shi and S. Z. D. Cheng, *Angew. Chem., Int. Ed.*, 2020, **59**, 18563–18571.
- 3 T. Qin, G. Zhou, H. Scheiber, R. E. Bauer, M. Baumgarten, C. E. Anson, E. J. W. List and K. Müllen, *Angew. Chem., Int. Ed.*, 2008, **47**, 8292–8296.
- 4 T. M. Figueira-Duarte and K. Müllen, *Chem. Rev.*, 2011, **111**, 7260–7314.

- 5 X. Cheng, T. Miao, L. Yin, Y. Ji, Y. Li, Z. Zhang, W. Zhang and X. Zhu, *Angew. Chem., Int. Ed.*, 2020, **59**, 9669–9677.
- 6 R. Zhang, X. Feng, R. Zhang, W. Shan, Z. Su, J. Mao, C. Wesdemiotis, J. Huang, X. Yan, T. Liu, T. Li, M. Huang, Z. Lin, A. Shi and S. Z. D. Cheng, *Angew. Chem., Int. Ed.*, 2019, **58**, 11879–11885.
- 7 B. Shao, S. Wan, C. Yang, J. Shen, Y. Li, H. You, D. Chen, C. Fan, K. Liu and H. Zhang, *Angew. Chem., Int. Ed.*, 2020, **59**, 18213–18217.
- 8 A. M. van de Craats, J. M. Warman, A. Fechtenkötter, J. D. Brand, M. A. Harbison and K. Müllen, *Adv. Mater.*, 1999, **11**, 1469–1472.
- 9 L. Zhi and K. Müllen, *J. Mater. Chem.*, 2008, **18**, 1472–1484.
- 10 D.-G. Kang, M. Park, D.-Y. Kim, M. Goh, N. Kim and K.-U. Jeong, *ACS Appl. Mater. Interfaces*, 2016, **8**, 30492–30501.
- 11 M. K. Smith and K. A. Mirica, *J. Am. Chem. Soc.*, 2017, **139**, 16759–16767.
- 12 D. Sheberla, L. Sun, M. A. Blood-Forsythe, S. Er, C. R. Wade, C. K. Brozek, A. Aspuru-Guzik and M. Dincă, *J. Am. Chem. Soc.*, 2014, **136**, 8859–8862.
- 13 T. Kambe, R. Sakamoto, T. Kusamoto, T. Pal, N. Fukui, K. Hoshiko, T. Shimojima, Z. Wang, T. Hirahara, K. Ishizaka, S. Hasegawa, F. Liu and H. Nishihara, *J. Am. Chem. Soc.*, 2014, **136**, 14357–14360.
- 14 M. G. Campbell, S. F. Liu, T. M. Swager and M. Dincă, *J. Am. Chem. Soc.*, 2015, **137**, 13780–13783.
- 15 Z.-Q. Yu, J. W. Y. Lam, K. Zhao, C.-Z. Zhu, S. Yang, J.-S. Lin, B. S. Li, J.-H. Liu, E.-Q. Chen and B. Z. Tang, *Polym. Chem.*, 2013, **4**, 996–1005.
- 16 D. Zeng, I. Tahar-Djebbar, Y. Xiao, F. Kameche, N. Kayunkid, M. Brinkmann, D. Guillon, B. Heinrich, B. Donnio, D. A. Ivanov, E. Lacaze, D. Kreher, F. Mathevet and A.-J. Attias, *Macromolecules*, 2014, **47**, 1715–1731.
- 17 I. Tahar-djebbar, F. Nekelson, B. Heinrich, B. Donnio, D. Guillon, D. Kreher and F. Mathevet, *Chem. Mater.*, 2011, **23**, 4653–4656.
- 18 M. Lehmann, M. Hecht, S. Herbst, K. Cui and F. Würthner, *Chem. Commun.*, 2020, **56**, 14015–14018.
- 19 M. Gupta, S. P. Gupta, M. V. Rasna, D. Adhikari, S. Dhara and S. K. Pal, *Chem. Commun.*, 2017, **53**, 3014–3017.
- 20 K.-U. Jeong, A. J. Jing, B. Mansdorf, M. J. Graham, D.-K. Yang, F. W. Harris and S. Z. D. Cheng, *Chem. Mater.*, 2007, **19**, 2921–2923.
- 21 K.-U. Jeong, A. J. Jing, B. Mansdorf, M. J. Graham, F. W. Harris and S. Z. D. Cheng, *J. Phys. Chem. B*, 2007, **111**, 767–777.
- 22 P. H. J. Kouwer and G. H. Mehl, *Angew. Chem., Int. Ed.*, 2003, **42**, 6015–6018.
- 23 P. H. J. Kouwer, J. Pourzand and G. H. Mehl, *Chem. Commun.*, 2004, 66–67.
- 24 Y. Shimizu, A. Kurobe, H. Monobe, N. Terasawa, K. Kiyohara and K. Uchida, *Chem. Commun.*, 2003, 1676–1677.
- 25 D. Tanaka, H. Ishiguro, Y. Shimizu and K. Uchida, *J. Mater. Chem.*, 2012, **22**, 25065–25071.
- 26 D. Tanaka, H. Ishiguro, T. Shirasu, D. Okuda, K. Uchida and Y. Shimizu, *Mol. Cryst. Liq. Cryst.*, 2014, **594**, 105–111.
- 27 Y. Chen, J. Lin, W. Yuan, Z.-Q. Yu, J. W. Lam and B. Z. Tang, *Sci. China: Chem.*, 2013, **56**, 1191–1196.
- 28 S.-J. Wang, R.-Y. Zhao, S. Yang, Z.-Q. Yu and E.-Q. Chen, *Chem. Commun.*, 2014, **50**, 8378–8381.
- 29 Z.-Q. Yu, J. W. Y. Lam, C. Zhu, E. Chen and B. Z. Tang, *Macromolecules*, 2013, **46**, 588–596.
- 30 Z.-Q. Yu, T.-T. Li, Z. Zhang, J.-H. Liu, W. Z. Yuan, J. W. Y. Lam, S. Yang, E.-Q. Chen and B. Z. Tang, *Macromolecules*, 2015, **48**, 2886–2893.
- 31 S. Z. D. Cheng, *Phase Transitions in Polymers: The Role of Metastable States*, Elsevier, 2008.
- 32 S. Paul, B. Ellman, S. Tripathi and R. J. Twieg, *J. Appl. Phys.*, 2015, **118**, 135702.
- 33 M. Al-Hussein, W. H. de Jeu, L. Vranichar, S. Pispas, N. Hadjichristidis, T. Itoh and J. Watanabe, *Macromolecules*, 2004, **37**, 6401–6407.
- 34 M. Yamada, A. Hirao, S. Nakahama, T. Iguchi and J. Watanabe, *Macromolecules*, 1995, **28**, 50–58.
- 35 S.-Y. Park, T. Zhang, L. V. Interrante and B. L. Farmer, *Macromolecules*, 2002, **35**, 2776–2783.
- 36 H. L. Xie, C. K. Jie, Z.-Q. Yu, X. B. Liu, H. L. Zhang, Z. Shen, E. Q. Chen and Q. F. Zhou, *J. Am. Chem. Soc.*, 2010, **132**, 8071–8080.
- 37 Y. Wu, L. H. You, Z.-Q. Yu, J.-H. Wang, Z. Meng, Y. Liu, X.-S. Li, K. Fu, X.-K. Ren and B. Z. Tang, *ACS Mater. Lett.*, 2020, **2**, 505–510.